Tarbiat Modares University

13th Iranian National Congress on Biosystems Engineering and Mechanization
15-17 September 2021

Iranian Society of Agricultural Machinery Engineering and Mechanization

Potential distribution and sensitivity map in ECT systems based on finite element method

Hossein Mousazadeh[a,*], Nazila Tarabi[b], , Jalil Taghizadeh-Tameh[b], Ali Kiapey[c], Farzad Mohammadi[d],

[a]Associate Prof., Mechanical Engineering of Biosystems, University of Tehran, Iran

[b]Ph.D. Candidate, Mechanical Engineering of Biosystems, University of Tehran, Iran

[c]Professional Researcher of Ports and Maritime Organization, Tehran, Iran

[d]Ph.D. student, Mechanical Engineering of Biosystems, University of Tehran, Iran

*Corresponding author: Department of Mechanical Engineering of Biosystems, University of Tehran, P.O. Box 4111, Karaj, Iran T: (98) 26 32801011
Email: hmousazade@ut.ac.ir

Abstract

Electrical capacitance tomography (ECT) is a non-invasive measurement technology, which is used to acquire spatial distribution information. It have application in many fields from food industry to oil and gas and especially to biomedical engineering and two-phase measurements. Defining potential distribution and sensitivity map is one of the primary problems associated to ECT systems. A computational procedure based on FEM is given in this text that could calculate the sensitivity in a short time. All derived equations are applied in a case study circular phantom and potential distribution and sensitivity maps are obtained respectively. The results show the robustness of the derived equations and sketched maps are shown good symmetry in circular medium.

Keywords; Electrical capacitance tomography, Finite element method, Sensitivity, Potential distribution, stiffness matrix.

1- Introduction

Electrical capacitance tomography (ECT) is a noninvasive imaging technique, which is used to acquire spatial distribution information from inaccessible objects in order to monitor industrial processes. ECT technology attempts to reconstruct the permittivity distribution of the cross-section via an appropriate reconstruction algorithm from the capacitance measurement data [1].

ECT has many potential applications in monitoring of two-phase permittivity application [2]. ECT systems have been extensively used in industry for monitoring non-conductive processes in oil, gas and chemical industries [3]. The concept of ECT was essentially evolved in 1980's as a novel method. The most successful application of ECT includes, imaging of gas/liquid mixture in oil pipeline, pneumatic conveying, fluidized beds and flame combustion [4].

Any ECT system consists of some electrodes usually in peripheral of a cylindrical phantom to measure capacitance in a designed pattern. The imaging algorithm consist of forward and inverse problems that defining the sensitivity map is essential for calculation.

In 2D analysis, the sensitivity distribution is essentially a map of the sensor response to a small individual area of high permittivity material in a low permittivity background as it positioned throughout the sensing area. Correspondingly, in 3D analysis, a small individual volume of high permittivity material in a low permittivity background as it positioned throughout the sensing volume.

The sensitivity distributions (or maps) can be obtained by physical measurement or by finite element (FE) analysis. There are several disadvantages difficult to overcome with the measurement method: (i) Many measurements are required; (ii) The test set up requires modification to investigate any change in physical parameters; (iii)The number of measurement points are rather limited for the test probe size must be big enough to ensure the capacitance changes are detectable;

(iv)It is very difficult to position a short test probe in a certain position in the 3D sensing field and not bring influence to the measurement. Consequently most investigators prefer the calculation method using a FE software package. The calculation of sensitivity maps is time consuming, especially in 3 dimension [5].

So, the main goal of this study is to introduce a sensitivity map generation methodology based on FEM. Discretization and modeling potential distribution is another object of this manuscript.

2-Materials and methods

Usually to most well-known approaches used for potential distribution calculation and sensitivity map derivation. These two approaches are Finite Element method (FEM) and Finite Difference Method (FDM). According to reviewed papers, The FEM-based calculation is definitely more complicated than FDM but provides good accuracy [6]. So this text is organized according to FEM for sensitivity map derivation.

2-1- Potential distribution based on FEM

The finite elements analysis of any problem involves basically four steps: (A) discretizing the solution region into a finite number of sub regions or elements, (B) deriving governing equations for a typical element, (C) assembling all the elements in the solution region, and (D) solving the system of equations obtained.

According to Fig. (1), discretization is dividing the whole region of interest in to some triangular or rectangular sections called element.

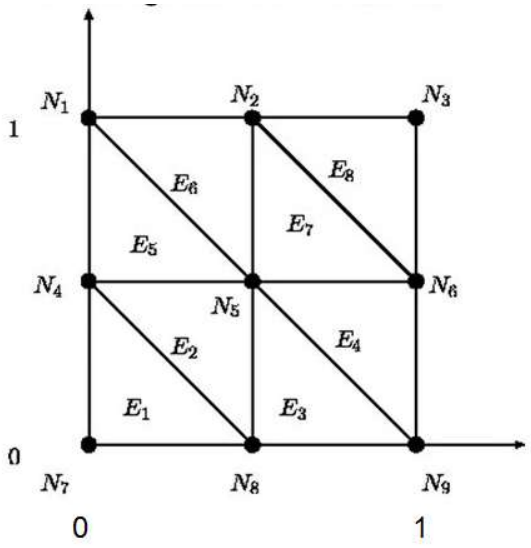

Fig 1) The area is discretized to 8 elements with 9 nodes

Since in ECT systems, Potential is applied in electrodes in the boundary, the aim is to seek an approximation for the potential, Ve within an element 'e' and then interrelate the potential distributions in various elements such that the potential is continuous across inter elements boundaries. The approximate solutions for the whole region is [7]:

$$V(x, y) = \sum_{e=0}^{N} V_e(x, y) \qquad (1)$$

Where N is the number of triangular elements into which the solution region is divided. The most common form of approximation for Ve, within an element is polynomial approximation, namely;

$$V_e(x,y)=a+bx+cy \qquad (2)$$

for triangular element and;

$$V_e(x,y)=a+bx+cy+dx\ y \qquad (3)$$

for a quadrilateral element. As assumption of linear variation of potential within the triangular elements is same as assuming that the electric field is uniform within the element.

The next step in FEM is deriving equations for an element. Considering a typical triangular element, as shown in Fig. (2).

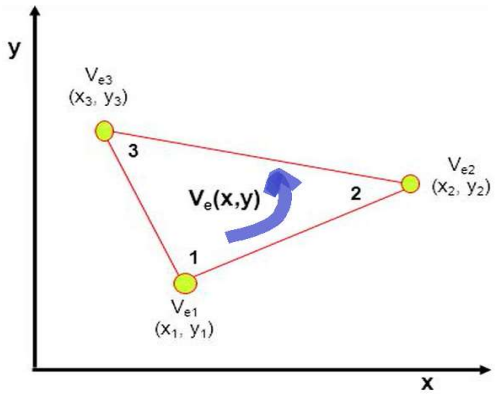

Fig 2) typical triangular element

The potential Ve1, Ve2 and Ve3 at nodes 1, 2, 3, respectively, are obtained by using Eq. (2); that is

$$\begin{bmatrix} Ve1 \\ Ve2 \\ Ve3 \end{bmatrix} = \begin{bmatrix} 1 & x_1 & y_1 \\ 1 & x_2 & y_2 \\ 1 & x_3 & y_3 \end{bmatrix} \begin{bmatrix} a \\ b \\ c \end{bmatrix} \quad (4)$$

The coefficients a, b, c is determined from above equation as:

$$\begin{bmatrix} a \\ b \\ c \end{bmatrix} = \begin{bmatrix} 1 & x_1 & y_1 \\ 1 & x_2 & y_2 \\ 1 & x_3 & y_3 \end{bmatrix}^{-1} \begin{bmatrix} Ve1 \\ Ve2 \\ Ve3 \end{bmatrix} \quad (5)$$

The inverse of a typical matrix A is defined as:

$$A^{-1} = \frac{1}{\det(A)} . Adj(A) \quad (6)$$

Where Adj(A) is adjugate of matrix A. But formula for the area of a triangle using determinants is as:

$$\text{Area} = \pm 1/2 \begin{vmatrix} x_1 & y_1 & 1 \\ x_2 & y_2 & 1 \\ x_3 & y_3 & 1 \end{vmatrix} \quad (7)$$

So; det(A) = |A| = 2* triangle_area = 2A

And;

$$\text{Adj(A)} = \text{Adj}(\begin{bmatrix} 1 & x1 & y1 \\ 1 & x2 & y2 \\ 1 & x3 & y3 \end{bmatrix}) \rightarrow A^T = \begin{bmatrix} 1 & 1 & 1 \\ x1 & x2 & x3 \\ y1 & y2 & y3 \end{bmatrix}$$

$$\text{Adj(A)} = \begin{bmatrix} x2.y3 - x3.y2 & x3.y1 - x1.y3 & x1.y2 - x2.y1 \\ y2 - y3 & y3 - y1 & y1 - y2 \\ x3 - x2 & x1 - x3 & x2 - x1 \end{bmatrix}$$

substituting this in Eq. (5) gives;

$$\begin{bmatrix} a \\ b \\ c \end{bmatrix} = \frac{1}{2.A} \begin{bmatrix} x2.y3 - x3.y2 & x3.y1 - x1.y3 & x1.y2 - x2.y1 \\ y2 - y3 & y3 - y1 & y1 - y2 \\ x3 - x2 & x1 - x3 & x2 - x1 \end{bmatrix} . \begin{bmatrix} Ve1 \\ Ve2 \\ Ve3 \end{bmatrix} \quad (8)$$

According to Eq. (2), where V(x,y) = a + b.x + c.y gives;

$$\text{V(x,y)} = [1 \ x \ y] \frac{1}{2.A} \begin{bmatrix} x2.y3 - x3.y2 & x3.y1 - x1.y3 & x1.y2 - x2.y1 \\ y2 - y3 & y3 - y1 & y1 - y2 \\ x3 - x2 & x1 - x3 & x2 - x1 \end{bmatrix} . \begin{bmatrix} Ve1 \\ Ve2 \\ Ve3 \end{bmatrix}$$

$$= \frac{1}{2.A} \begin{bmatrix} (x2.y3 - x3.y2) + (y2 - y3)x + (x3 - x2)y \\ (x3.y1 - x1.y3) + (y3 - y1)x + (x1 - x3)y \\ (x1.y2 - x2.y1) + (y1 - y2)x + (x2 - x1)y \end{bmatrix}^T . \begin{bmatrix} Ve1 \\ Ve2 \\ Ve3 \end{bmatrix} \quad (9)$$

So, V(x, y), potential in any point of element is as;

$$\text{V(x, y)} = \sum_{i=1}^{3} \alpha_i(x, y) V_{ei} \quad (10)$$

The value of A is positive if the nodes are numbered counterclockwise. Above equation gives the potential at any point within the element, provided the potentials at the vertices are known. Where αi is given as [7];

$$\left\{\begin{array}{l}\alpha 1=\frac{1}{2.A}(x2.y3-x3.y2)+(y2-y3)x+(x3-x2)y\\ \alpha 2=\frac{1}{2.A}(x3.y1-x1.y3)+(y3-y1)x+(x1-x3)y\\ \alpha 3=\frac{1}{2.A}(x1.y2-x2.y1)+(y1-y2)x+(x2-x1)y\end{array}\right\} \quad (11)$$

So in terms of nodal coordinates, the Potentail *Yij,* between node *i* and node *j* is determined by the triangle-to-network conversion as

[8], [7], [9], [10];

$$Y_{ij}=\frac{\varepsilon_r}{4A_e}(b_ib_j+c_ic_j),(i\neq j) \quad (12)$$

with *b1= y2- y3, b2= y3 – y1, b3 = y1 – y2 and c1 = x3 – x2, c2 = x1 – x3, c3 = x2 – x1.* Where *(xi, yi) (i* = 1,2,3) denotes a coordinate of each node. Ae indicates the area of an element and ε_r is the element permittivity.

With Y11 = - Y12 – Y13, Y22 = - Y21 – Y23, Y33 = -Y31 – Y32, Yij = Yji.

Stiffness matrix for a typical element, e, shown in the Fig. (3), given as [8];

$$Y^e=\begin{bmatrix}Y_{11}^e & Y_{12}^e & Y_{14}^e\\ Y_{21}^e & Y_{22}^e & Y_{24}^e\\ Y_{41}^e & Y_{42}^e & Y_{44}^e\end{bmatrix} \quad (13)$$

The third step in FEM is assembling all the elements. The two element mesh of Fig. (3) is used to illustrate the assembling of the global admittance matrix. The master matrix Y is assembled with the permittivity between adjacent elements adding in parallel as in Fig. (3). These two elements share nodes 2 and 4, however *Y24* will be different

for each triangle since the permittivity, ε, and the geometry is different for each element.

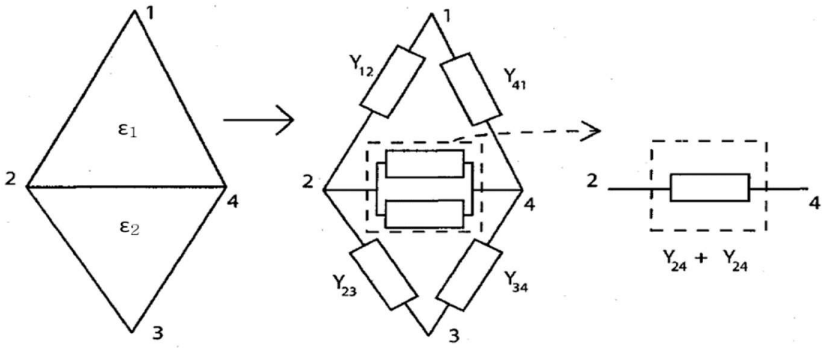

Figure 3) Connection of two elements

For the mesh of Fig. (3), the local matrices are:

$$Y_{ij}^{(1)} = \begin{bmatrix} Y_{11} & Y_{12} & Y_{14} \\ Y_{21} & Y_{22} & Y_{24} \\ Y_{41} & Y_{42} & Y_{44} \end{bmatrix}$$

i,j ∈ [1, 2, 4] are the global node indices for element 1

$$Y_{ij}^{(2)} = \begin{bmatrix} Y_{22} & Y_{23} & Y_{24} \\ Y_{32} & Y_{33} & Y_{34} \\ Y_{42} & Y_{43} & Y_{44} \end{bmatrix}$$

i,j ∈ [2, 3, 4] are the global node indices for element 2

These two matrixes are combined as follows;

$$\mathbf{Y} = \begin{bmatrix} Y_{11} & Y_{12} & Y_{13} & Y_{14} \\ Y_{21} & Y_{22}+Y_{22} & Y_{23} & Y_{42}+Y_{42} \\ Y_{31} & Y_{32} & Y_{33} & Y_{34} \\ Y_{41} & Y_{42}+Y_{42} & Y_{43} & Y_{44}+Y_{44} \end{bmatrix} \quad i,j \in [1:4]$$

All of discretized elements in the cross-sectional area are assembled accordingly to form the global admittance matrix. Therefore for Fig. (1), the global admittance matrix would be a square 8*8 matrix. In large global admittance matrixes, most arrays are zero.

The final step in FEM is solving the resulting equations. The energy associated with the assemblage of all elements in the mesh is [7]:

$$W=\sum_{e=1}^{N} W_e=\frac{1}{2}\varepsilon\,[V]^T[C][V] \qquad (14)$$

and

$$[V]=\begin{bmatrix} V_1 \\ \vdots \\ V_n \end{bmatrix} \qquad (15)$$

where n is the number of nodes, N is the number of elements, and [C] is called the overall or global coefficient matrix (it is shown by 'Y' in some texts), which is the assemblage of individual element coefficient matrices.

If all free nodes are numbered first and the fixed nodes last, Eq. (14) can be written such that;

$$W=\frac{1}{2}\varepsilon[V_f \quad V_p]\begin{bmatrix} c_{ff} & c_{fp} \\ c_{pf} & c_{pp} \end{bmatrix}\begin{bmatrix} V_f \\ V_p \end{bmatrix} \qquad (16)$$

Where subscripts f and p, respectively, refer to nodes with free (nodes that their potential is unknown) and fixed (or prescribed or nodes with defined potential in boundary) potentials. Since Vp is constant, we differentiate only With respect to Vf, yields;

$$W=\frac{1}{2}\,\varepsilon\,[Vf \quad Vp].\begin{bmatrix} Cff.Vf+Cfp.Vp \\ Cpf.Vf+Cpp.Vp \end{bmatrix}$$

$$=\frac{1}{2}\,\varepsilon\,\left(Vf.(Cff.Vf+Cfp.Vp)+Vp.(Cpf.Vf+Cpp.Vp)\right)$$

$$\frac{\partial W}{\partial(Vf,Vp)}=0\;\rightarrow\;Cff.Vf+Cfp.Vp=0\;\rightarrow[Cff][Vf]=-[Cfp][Vp] \qquad (17)$$

This can be written as;

$$[A][V]=[B]$$

$$[V]=[A]^{-1}[B] \qquad (18)$$

where [A] = [Cff], [V] = [Vf] and [B] = − [Cfp][Vp]

Since [A] is, in general, non-singular, the potential at the free nodes can be found by using Eq. (9). The "1/2" is removed from two sides of equation (18) when differentiation.

2-2- Sensitivity map generation

To generate 2D sensitivity map based on the earlier calculations, a cylindrical phantom is considered as a desired medium. The cross-sectional area of this phantom is discretized to 576 elements as shown in the Fig. (4) with 8 electrodes on the perimeter.

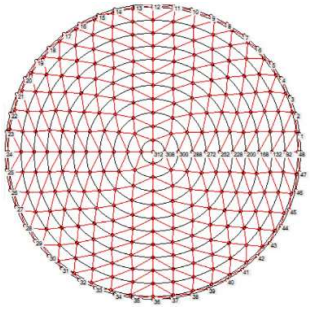

Figure 4) Discretization of phantom cross-section

In soft-field tomography (e.g. ECT), sensitivity maps need to be generated before imaging [11]. The most useful form is to produce the capacitance readings of each electrode pair when a single test pixel of high permittivity is moved to cover the whole imaging area against a low permittivity background. Capacitance sensitivity distributions (i.e. sensitivity maps) for each electrode pair can be produced from these data [12]. There are two principal methods of obtaining the data:

(1) Based on physical capacitance measurements

(2) By iterative calculations based on potential distributions.

The first method (experimental) is based on placing a test object at each pixel position in turn and measuring the resultant change in capacitance of each electrode pair.

Because the definition of the sensitivity-map is the permittivity change in each element causing the change in capacitance, the function is given by:

$$S_{i,j}(k) = \frac{C_{i,j}^{k} - C_{i,j}^{L}}{\left(C_{i,j}^{H} - C_{i,j}^{L}\right)\left(\varepsilon_H - \varepsilon_L\right)} \frac{A}{A(k)} \qquad (19)$$

where $S_{ij}(k)$ is the sensitivity of each element, ε_H and ε_L are the permittivity values with higher and lower permittivity medium, $C^{k}_{i,j}$ is the capacitance measurement from k^{th} element with higher permittivity, but all others elements with lower permittivity, $C^{H}_{i,j}$, means the capacitance value with all elements having higher permittivity, $C^{L}_{i,j}$ is similar to $C^{H}_{i,j}$ but with lower permittivity, A is the cross section of the sensor and $A(k)$ is the area of each pixel.

The second method is to use the potential distributions E = -grad(ϕ(x,y)) to calculate the sensitivity-map. When a voltage Vi is applied to the i^{th} electrode, the potential distributions are computed using FEM/FDM. For an 8-electrode sensor, the capacitance Cij between the ith and jth in electrode pair can be calculated from the field distributions and finally the sensitivity-map Si,j(x,y) can be obtained by an approximation method, expressed by equation (20) in gradient format of electric field in Laplace equation:

$$S_{i,j}(x,y) = -\oint_{p(x,y)} \frac{E_i(x,y)}{V_i} \cdot \frac{E_j(x,y)}{V_j} dxdy$$

$$S_{i,j}(x,y) = -\frac{1}{\mathrm{Vi.Vj}} \oint_{p(x,y)} \left(\frac{\partial \phi_i}{\partial x} \cdot \frac{\partial \phi_j}{\partial x} + \frac{\partial \phi_i}{\partial y} \cdot \frac{\partial \phi_j}{\partial y} \right) dxdy \qquad (20)$$

where ∂ϕi/∂x is the gradient value of potential $Ei(x,y)$ with electrode i in X vector, and ∂ϕi/∂y is the gradient value of potential $Ei(x,y)$ with electrode i in Y vector. The gradient values of potential $Ei(x,y)$ are ∂ϕj/∂x and ∂ϕj/∂y [13].

For all excitations the distribution of the potentials is computed by FEM, and then, in the centre of every pixel of the map the vector **E** is found using E= -grad V. The electric field intensity vectors for every case of excitation are stored and then used to compute the sensitivities. The number of rows in the sensitivity matrix S is equal to the number of the mutual capacitances $N = n(n-1)/2$. The number of columns of S is equal to k – the number of pixels in the image, as given in [14] and [15].

So, to calculate the sensitivity matrix, potential in any point of element is calculated from Eq. (10);

$$\frac{\partial \emptyset i}{\partial x} = \frac{1}{2A}\left((y2-y3).V_1^{ei} + (y3-y1).V_2^{ei} + (y1-y2).V_3^{ei}\right)$$

$$\frac{\partial \emptyset i}{\partial y} = \frac{1}{2A}\left((x3-x2).V_1^{ei} + (x1-x3).V_2^{ei} + (x2-x1).V_3^{ei}\right) \qquad (21)$$

where $V^{ei}{}_1$, $V^{ei}{}_2$ and $V^{ei}{}_3$ are potential at nodes 1, 2 and 3 of element 'e' when i^{th} electrode is as source and last electrodes are sink.

$$S_{i,j}(x,y) = \frac{-1}{Vi.Vj}\oint_{p(x,y)} \begin{bmatrix} \frac{1}{2A}\left((y2-y3).V_1^{ei} + (y3-y1).V_2^{ei} + (y1-y2).V_3^{ei}\right) * \\ \frac{1}{2A}\left((y2-y3).V_1^{ej} + (y3-y1).V_2^{ej} + (y1-y2).V_3^{ej}\right) + \\ \frac{1}{2A}\left((x3-x2).V_1^{ei} + (x1-x3).V_2^{ei} + (x2-x1).V_3^{ei}\right) * \\ \frac{1}{2A}\left((x3-x2).V_1^{ej} + (x1-x3).V_2^{ej} + (x2-x1).V_3^{ej}\right) \end{bmatrix} dx\,dy$$

$$= \frac{-1}{4A.Vi.Vj}\begin{bmatrix} \left((y2-y3).V_1^{ei} + (y3-y1).V_2^{ei} + (y1-y2).V_3^{ei}\right) * \\ \left((y2-y3).V_1^{ej} + (y3-y1).V_2^{ej} + (y1-y2).V_3^{ej}\right) + \\ \left((x3-x2).V_1^{ei} + (x1-x3).V_2^{ei} + (x2-x1).V_3^{ei}\right) * \\ \left((x3-x2).V_1^{ej} + (x1-x3).V_2^{ej} + (x2-x1).V_3^{ej}\right) \end{bmatrix} \qquad (22)$$

After derivation of sensitivity matrix it would be normalized to reduce noise impacts in any conditions. The normalized sensitivity matrix S can be calculated from matrix s as follow.

$$S_{mn} = \frac{s_{mn}}{\sum_{n=1}^{M} s_{mn}} \qquad (23)$$

where S_{mn} and s_{mn} denote the elements in the m^{th} row and the n^{th} column of N ×M matrix S and N ×M matrix s, respectively [16]. Actually the denominator is sum of each row.

All simulations including; region discretizing, potential distribution maps and sensitivity maps derivation are performed in an application program, written in C#.

3-Results and discussions

To evaluate the system response and to derive potential distribution and sensitivity map, it is applied 1 volts on incentive electrode and all the other electrodes are grounded by 0 volts.

The simulation of single-plane sensor will help to analyze the derived equations in the last section. The permittivity distribution in the simulations is selected to suit the experimental setup. Approximately 4 mm is considered as pipe thickness and the remaining area is considered as a phantom with internal diameter of about 200 mm. One outer layer elements that is considered as pipe, are taken with permittivity of εr=3. Three mediums were simulated within the sensing zone; first sensing region considered with air i.e. empty pipe (εr = 1), second it is considered to be full filled with typical cereal (εr = 5) and third with deionised water (εr = 80) respectively. Fig. 5 depicts the electrical field distribution of single excited electrode in case for 2D simulation. It specifies that the area which is closer to the electrode possess high voltage and intense equipotential regions. From the post processing result, the potential and media distribution has been obtained on the

sensitive field of the sensing region as shown in Fig. 5(a), 5(b) and 5(c) subsequently.

The result demonstrates the distribution of potential i.e. 1 V at only single energized electrode and leftover retaining at zero potential (i.e. ϕ = 0V). From the figure, blue color signifies the region with no potential (near to zero). However, the area with distinct colors denotes the sensing region with diverse electric potential (i.e. where the field can be sensitive). A region close to a source electrode depicts a significant distribution of potential.

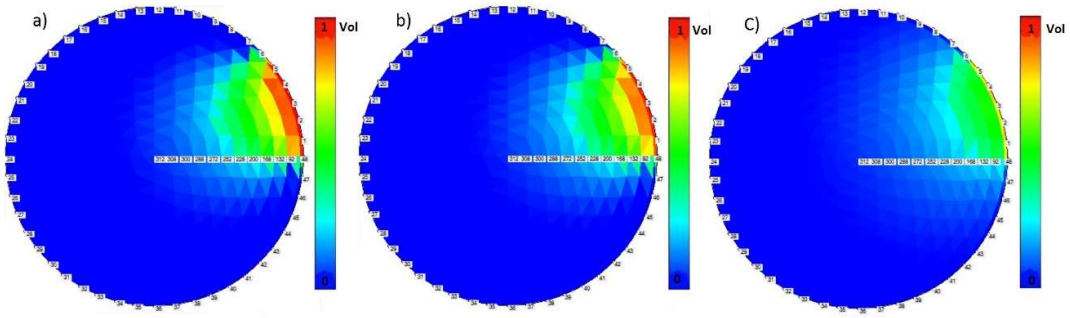

Figure 5) Potential distribution map when the electrode 1 is as source electrode and (a) εr=1, (b) εr=5, (c) εr=80.

To obtain sensitivity map of ECT system, the high permittivity is considered as ε_{high}=5 and the background or low permittivity as air, ε_{low}=1. Figure (6) shows the sensitivity map for some electrode pairs.

From this figure, we can see that the sensitivity value for adjacent electrode pair 1-2 is very high. For the other electrode pairs 1-3, 1-4 and 1-5, 1-6, 1-7 and 1-8 the sensitivity is high near the frame wall, while the sensitivity shows negative values far from the path between two electrodes. The sensitivity value is normalized before drawing as a map. In the Fig. (6), the sensitivity is illustrated only when one of electrodes is electrode 1. However, this process will be repeated for each electrode until all 28 projections are measured. As a result, the electric field distribution of the projection beam from one sensor to another will be intensified as in Fig. (6). It shows the generated sensitivity map for the permittivity distribution for electrode e1-e5, …,

and e1-e8. Other sensitivity maps that are not shown here, will be similar to one of these seven illustrated maps.

The other projections from an excitation electrode *ei* to the detectors *ej* are not depicted here. Since the circular electrode positions are symmetrical, only 28 independent projections are required.

From Fig. (6), it is observed that the sensitivity field is non-uniformly distributed over the medium of interest. The sensitivity is higher within the area closer to the excitation and detection electrode pair. On the other hand, its sensitivity is much lower in the center region. Therefore, the drawback of this soft-field effect will affect the measurements on the center region.

Sensitivity matrix consists some positive and negative numbers as well as. According to Fig. (6), all positive and negative numbers are illustrated continuously by a color column from red to blue.

Depending on discretized element numbers and electrode numbers as well, the sensitivity map computing is very time consuming procedure, especially in 3D ECT. However, although increasing number of elements inside phantom, would increase precision and resolution of image, but it would cause very high processing load on the PC's CPU. This would be an important problem in online cases.

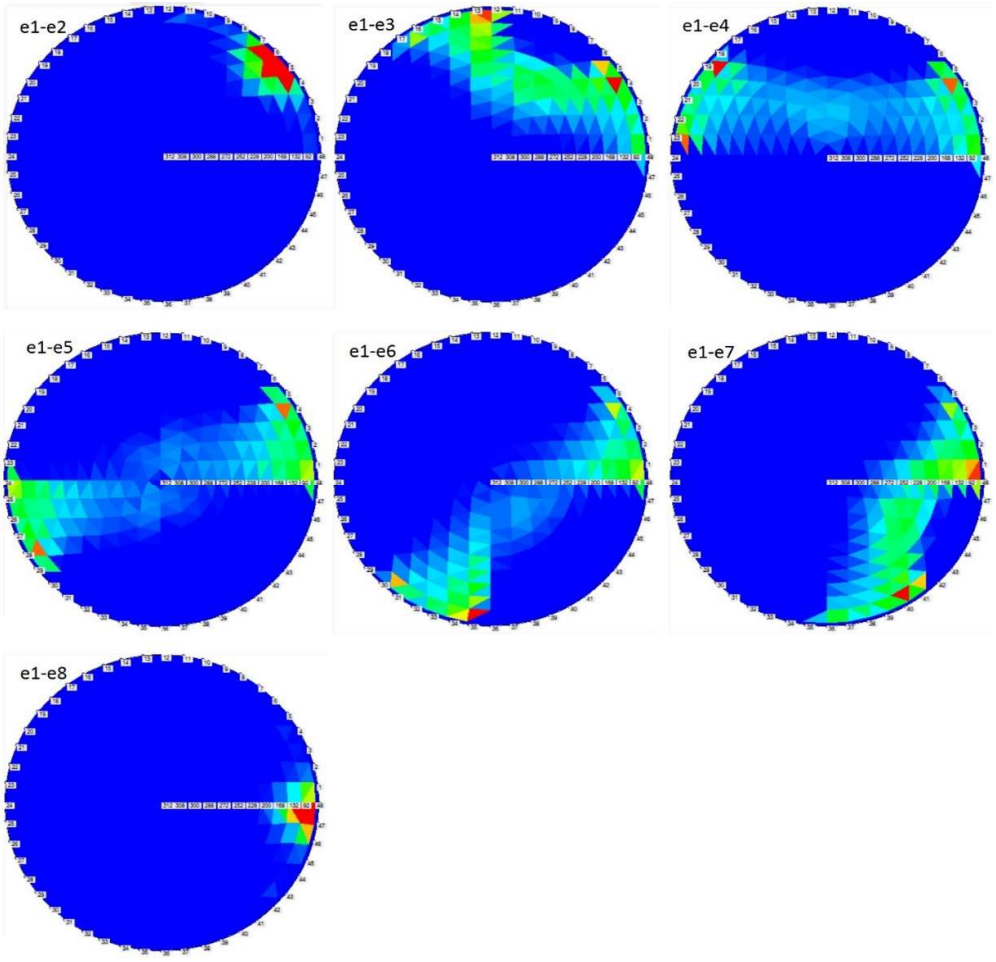

Figure 6) Sensitivity map for electrode pairs of e1-ei (2≤i≤8).

4-Conclusion

ECT based measurement systems are non-invasive instruments and have application in many fields from food industry to oil and gas and two-phase measurements. Defining potential distribution and sensitivity map is one of the primary problems associated to ECT systems. A computational procedure based on FEM is given in this text that could calculate the sensitivity in a short time. All derived equations are applied in a case study circular phantom and potential distribution and sensitivity maps are obtained respectively. The results show the robustness of the

derived equations and sketched maps are shown good symmetry in circular medium.

Acknowledgment

Authors would like to acknowledge the Ports and Maritime Organization for funding the project by grant No. 6668/S20, 2020-2022.

References

[1] Jing Lei, Shi Liu, Xueyao Wang and Qibin Liu. 2013. An Image Reconstruction Algorithm for Electrical Capacitance Tomography Based on Robust Principle Component Analysis. doi:10.3390/s130202076.

[2] M. Soleimani and A. Movafeghi. 2005. Electrical permittivity shape identification using electrical capacitance tomography data and level set formulation. The third conference on machine vision, image processing & application, Tehran, Iran.

[3] Saied I, Meribout M. 2016. Electronic hardware design of electrical capacitance tomography systems. *Phil. Trans. R. Soc. A* 374: 20150331.

[4] S. M. Huang, A. B. Plaskowski, C. G. Xie, and M. S. Beck, "Tomographic imaging of two-component flow using capacitance sensors," Journal of Physics E: Scientific Instruments, vol. 22, 1989, p. 173.

[5] Hua Yan, Fuqun Shao, and Shi Wang. 1999. 1st Word Congress on Industrial Tomography, Buxton, Greater Manchester, April 14-17,. Simulation Study of Capacitance Tomography Sensors.

[6] Mimi Faisyalini Ramli. 2017. Multiphase Flow Measurement with Electrical Capacitance Tomography and Microwave Sensors. Thesis submitted to The University of Manchester for the degree of Doctor of Philosophy.

[7] Biswanath Malik. 2009. Electric field calculations by numerical techniques. A thesis submitted in fulfillment of the requirements for the degree of bachelor of technology. Department of electrical engineering national institute of technology Rourkela.

[8] Bradley Michael Graham. 2007. Enhancements in EIT Image Reconstruction for 3D Lung Imaging. Thesis submitted to the Faculty of Graduate and Postdoctoral Studies In partial fulfillment of the requirements For the PhD degree in Electrical and Computing Engineering.

[9] Finite Element Method. Accessed at; 2021. Accessed in; https://slidetodoc.com/finite-element-method-fem-approaches-there-are-two/

[10] Pan Jiang, Shidong Fan, Ting Xiong, Haofei Huang . Investigation on the Sensitivity Distribution in Electrical Capacitance Tomography System. TELKOMNIKA, Vol. 11, No. 12, December 2013, pp. 7088~7093 .

[11] Jerbi K, Lionheart W R B, Yauhkonen P J and Yauhkonen M. 2000. Sensitivity matrix and reconstruction algorithm for EIT assuming axial uniformity. *Physiol. Meas.,* 21, pp 61-66.

[12] Yang W Q and Conway W F. 1998. Measurement of sensitivity distributions of capacitance tomography sensors. *Rev. Sci. Instrum.,* 69 (1), pp 233-236

[13] Yi Li. 2008. Key issues of 2D/3D image reconstruction in electrical tomography. A thesis submitted to The University of Manchester for the degree of Doctor of Philosophy.

[14] Kostadin Brandisky, Andrzej Romanowski, Krzysztof Grudzien and Dominik Sankowski. 2010. Electrostatic Field Simulations in the Analysis and Design of electrical capacitance tomography sensors. Automatyka. Tom 14, Zeszyt 3/2. 655- 669.

[15] Xiangyuan Dong and Shuqing Guo. 2013. Analytical Method of Generating Sensitivity Map for Electrical Capacitance Tomography

Sensor with Internal Electrode. *doi:10.4028/www.scientific.net/AMM.339.99*

[16] Hua Yan, Yan Hui Sun, Yi Fan Wang, Ying Gang Zhou. 2015. Comparisons of three modelling methods for the forward problem in three-dimensional electrical capacitance tomography. IET Sci. Meas. Technol., Vol. 9, Iss. 5, pp. 615-620.